Angular power spectrum of the FASTICA cosmic microwave background component from Background Emission Anisotropy Scanning Telescope data

S. Donzelli,[1,2]* D. Maino,[1] M. Bersanelli,[1] J. Childers,[3] N. Figueiredo,[4] P. M. Lubin,[3] P. R. Meinhold,[3] I. J. O'Dwyer,[5] M. D. Seiffert,[6] T. Villela,[7] B. D. Wandelt[5] and C. A. Wuensche[7]

[1]*Dipartimento di Fisica, Università di Milano, Via Celoria 16, 20133 Milano, Italy*
[2]*SISSA/ISAS, Astrophysics Sector, Via Beirut 4, 34014 Trieste, Italy*
[3]*Physics Department, University of California, Santa Barbara, CA 93106, USA*
[4]*Universidade Federal de Itajubá, Departamento de Física e Química, Caixa Postal 50, 37500-903, Itajubá, MG, Brazil*
[5]*Astronomy Department, University of Illinois at Urbana-Champaign, Urbana, IL 61801-3074, USA*
[6]*Jet Propulsion Laboratory, Oak Grove Drive, Pasadena, CA 91109, USA*
[7]*Instituto Nacional de Pesquisas Espaciais, Divisão de Astrofísica, Caixa Postal 515, 12245-970, São José dos Campos, SP, Brazil*

ABSTRACT

We present the angular power spectrum of the cosmic microwave background (CMB) component extracted with FASTICA from the Background Emission Anisotropy Scanning Telescope (BEAST) data. BEAST is a 2.2-m off-axis telescope with a focal plane comprising eight elements at *Q* (38–45 GHz) and *Ka* (26–36 GHz) bands. It operates from the UC (University of California) White Mountain Research Station at an altitude of 3800 m. The BEAST CMB angular power spectrum has already been calculated by O'Dwyer et al. using only the *Q*-band data. With two input channels, FASTICA returns two possible independent components. We found that one of these two has an unphysical spectral behaviour, while the other is a reasonable CMB component. After a detailed calibration procedure based on Monte Carlo (MC) simulations, we extracted the angular power spectrum for the identified CMB component and found a very good agreement with the already published BEAST CMB angular power spectrum and with the *Wilkinson Microwave Anisotropy Probe* (*WMAP*) data.

Key words: methods: data analysis – techniques: image processing – cosmic microwave background.

1 INTRODUCTION

The recent outstanding results from *Wilkinson Microwave Anisotropy Probe* (*WMAP*) satellite (Bennett et al. 2003) have definitely put us into the era of precision cosmology with an accurate determination of the cosmic microwave background (CMB) angular power spectrum up to $\ell \simeq 800$. In addition, the Degree Angular Scale Interferometer (DASI) experiment (Leitch et al. 2005) has clearly reported detection of *E*-mode CMB polarization. The situation will improve even further with the *Planck* satellite, a third generation CMB space mission which will map microwave emission over the whole sky with an unprecedented combination of angular resolution and sensitivity. In the meantime, a plethora of both ground-based and balloon-borne experiments will produce accurate measurements (better than *WMAP*) over limited sky regions.

Today, one of the main limitations to the accuracy is the presence of other astrophysical sources between us and the last scattering surface, which contribute to the measured signal. These foreground contaminants consist mainly of Galactic emission (synchrotron, free–free and dust emission), compact galactic and extragalactic sources and the Sunyaev–Zel'dovich effect from cluster of galaxies. The challenge is to identify and remove such foreground emissions with high accuracy and reliability in order to obtain cleaned CMB maps. This is crucial in deriving precise cosmological information from the CMB power spectrum.

Many works have been dedicated to component separation, and different algorithms have been proposed. Traditional separation techniques, from Wiener filtering (Tegmark & Efstathiou 1996; Bouchet et al. 1999; Prunet et al. 2001) to maximum entropy method

*E-mail: simona.donzelli@mi.infn.it

(MEM) (Hobson et al. 1998; Stolyarov et al. 2002), have generally been employed. They achieve good results, but they require prior knowledge about the signals to be separated (e.g. spatial templates and frequency dependence), whereas the available full-sky foreground priors actually are not completely reliable.

Recently, a blind separation approach has been developed, which works without the need of priors, except about the statistical features of the components. Indeed, this technique, based on the Independent Component Analysis (ICA) (Comon 1994), exploits the statistical independence of the sky signals. It was first implemented as a neural network (Baccigalupi et al. 2000), and then optimized in a fast algorithm, FASTICA (Maino et al. 2002), which was successfully tested on simulated sky maps similar to those that *Planck* will produce. FASTICA has shown good performance also when applied to real data from *COBE*-DMR (Differential Microwave Radiometer; Maino et al. 2003), with results on CMB anisotropy and foreground contamination consistent with previous and independent analyses.

In this work, we apply FASTICA to another real data set, from the Background Emission Anisotropy Scanning Telescope (BEAST). In Section 2, we briefly recall the main features of the FASTICA approach and its assumptions. In Section 3, after describing the BEAST instrument and the maps produced, we explain the procedure followed to apply FASTICA to BEAST data. The results obtained are presented in Section 3.1, and the CMB reconstruction quality, tested with Monte Carlo simulations, is analysed in Section 3.2. Section 4 deals with the normalization of the CMB signal extracted with FASTICA. In Section 5, we extract the FASTICA CMB spectrum. Finally, a critical discussion and conclusions are presented in Section 6.

2 COMPONENT SEPARATION WITH FastICA

Before describing the FASTICA method, it is useful to recall briefly the data model FASTICA refers to and the principal assumptions from which it derives, described in detail in Maino et al. (2002).

Let us suppose that the sky radiation, as a function of direction r and frequency ν, is a superposition of N different signals $s_j(r, \nu)$ and that it is observed by an experiment with M frequency channels whose beam pattern is $B(r, \nu)$. Let us further suppose that, for each signal, frequency and spatial dependence can be factored into two separated terms, $f_j(\nu)$ and $\bar{s}_j(r)$, respectively, and that B is shift invariant and frequency independent. Then, the data model can be written as

$$x(r) = A\bar{s}(r) * B(r) + \epsilon(r) = As(r) + \epsilon(r), \tag{1}$$

where each component, s_j, of the vector s is the corresponding source function convolved with the B beam pattern. The matrix A is the mixing matrix, which includes the frequency response, and $\epsilon(r)$ is the instrumental noise term.

The FASTICA algorithm obtains both the mixing matrix A and the signals s from observed data x assuming that

(i) the signals s are independent random processes on the map domain;

(ii) all the signal, but at most one, have non-Gaussian distribution.

A detailed explanation of this strategy can be found in Hyvärinen & Oja (1997) and Hyvärinen (1999), while its application in an astrophysical context is described in Maino et al. (2002). Independent components are extracted maximizing a suitable measure of non-Gaussianity that is robust against noise; this is the so-called neg-entropy.

FASTICA estimates separation matrix W row by row, maximizing the non-Gaussianity of the component $w^T\hat{x}$, where w^T is a row of W, such that the transformed variables $y = Wx$ are the independent components.

In particular, the FASTICA algorithm operates with a neg-entropy approximation (Hyvärinen 1999; Hyvärinen & Oja 2000), which can assume three different forms, depending on the regular non-quadratic function chosen in its expression: $g(u) = u^3, g(u) = u \exp(-u^2)$ or $g(u) = \tanh(u)$, where $u = w^T\hat{x}$. In the following, we indicate these functions as p, g and t, respectively. The best choice of the function depends on the statistical proprieties of the components: kurtosis, or p, can be used for sub-Gaussian components in the absence of outliers; g may be better when the components are highly super-Gaussian or when robustness is important; t is a general-purpose function (Hyvärinen 1999). However, we do not know a priori the statistics of the independent signals.

Once the separation matrix W is obtained, since we have $x = W^{-1}y$, we can derive the frequency scalings for each independent component; the scaling between ν and ν' of the jth component is given by the ratio of $W_{\nu j}^{-1}/W_{\nu' j}^{-1}$. If the spectral behaviour is given by a power law with index β, then we have $\beta = \log(W_{\nu j}^{-1}/W_{\nu' j}^{-1})/\log(\nu/\nu')$. Therefore, a negative value of frequency scaling indicates that the recovered component does not have a physical behaviour.

Furthermore, we can estimate the noise in the reconstructed maps. If we perform noise-constrained realizations n_x for each frequency channel, the corresponding noise realizations in the FASTICA outputs are given by Wn_x.

3 APPLICATION TO BEAST DATA

The BEAST is a 2.2-m off-axis Gregorian telescope (Figueiredo et al. 2005) with a focal plane consisting of six Q band (38–45 GHz) and two Ka band (26–36 GHz) corrugated scalar feed horns coupled with cryogenic High Electron Mobility Transistor (HEMT) amplifiers (Childers et al. 2005). The instrument was installed at the UC White Mountain Research Station at an altitude of 3.8 km in 2001 July. Data considered here come from two different campaigns: one until 2001 December and the other in 2002 (February and August/September).

BEAST produced two maps covering an annular sky region around the Nord Celestial Pole (NCP) from $33° < \delta < 42°$ with a resolution of 23 arcmin in Q band and 30 arcmin in Ka band. The sky maps are pixelized according to the HEALPix (Hierarchical Equal Area isoLatitude Pixelization)[1] scheme (Górski, Hivon & Wandelt 1999) with a resolution parameter $N_{\rm side} = 512$ corresponding to a pixel size of 6.9 arcmin.

For a proper analysis of the results that FASTICA will obtain, we need to know the instrumental noise properties, namely noise level in the two frequency bands and its spatial distribution. To estimate instrumental noise, Meinhold et al. (2005) have made 'difference' maps at the two frequency bands separately. They binned data from first half of observation into one map and the second half into the other. For each band, the 'difference' map is the pixel-by-pixel difference of these two maps, divided by 2 to maintain noise statistics as in the sum map. Therefore, these maps should not contain in principle any sky signal, but only noise and the rms of these maps is a measure of instrumental noise. The signal-to-noise ratio (S/N) is quite poor: for the Q-band map Meinhold et al. (2005) have found a value $\sim$0.11 at 23-arcmin resolution, which becomes $\sim$0.57 when

[1] See http://www.eso.org/science/healpix/

Table 1. ICA frequency scaling of the astrophysical component from BEAST maps smoothed at the three angular resolution, and for the three Galactic cuts.

Resolution	$|b| \leqslant 17.5°$			$|b| \leqslant 20°$			$|b| \leqslant 22°$		
	p	g	t	p	g	t	p	g	t
30′	0.221	0.129	2.382	0.190	0.118	2.470	0.177	0.068	2.480
40′	0.127	1.296	2.683	1.459	1.116	3.036	1.580	1.090	2.838
60′	1.049	1.148	2.917	0.927	$-^a$	3.141	0.930	0.815	2.928

^{a}No convergence of the FASTICA algorithm.

the map is smoothed at 30 arcmin. The *Ka*-band map shows a higher noise contribution. In addition, from the 'difference' maps we can see that noise is Gaussian but, due to the scanning strategy, is not uniformly distributed on the sky.

Before applying FASTICA a smoothing of the maps is required, due to the different angular resolution in the two bands, since in FASTICA approach it is assumed a frequency-independent beam pattern (see equation 1). We have smoothed the *Ka* and the *Q* maps to the same angular resolution, choosing values of 30, 40 and 60 arcmin in order to increase the S/N ratio. To obtain maps with significant signal level, we decided not to smooth to resolution greater than 60 arcmin, because of the 10-Hz high-pass filter applied to the BEAST data in the reduction processing; this indeed produces a signal cut-off on angular scales $\gtrsim 6°$.

We applied FASTICA to the BEAST maps at the three resolutions working with all the non-quadratic functions described before identified by *p*, *g* and *t*, respectively. With two input sky maps, FASTICA is able to reconstruct only two outputs, since the estimated matrix **W** has dimension 2×2. For all the considered cases, one of the two is an astrophysical component, while the second component, due to the low-S/N ratio, always has a negative frequency scaling, which suggests unphysical behaviour as explained in the previous section. Performing a component separation on the full observed sky, FASTICA recovers an astrophysical signal with a frequency scaling consistent with free–free emission. This is due to the strong Galactic emission in the two plane crossings. Therefore, in order to reconstruct the CMB component, we cut the sky regions where foreground emission overcomes CMB. We remove the three strongest point sources and the Galactic plane, cutting out data within three different values of Galactic latitude: $|b| \leqslant 17.5°$, $|b| \leqslant 20°$ and $|b| \leqslant 22°$. Mejía et al. (2005) have estimated that, removing from BEAST maps regions with $|b| \leqslant 17.5°$, the individual Galactic contributions remain below ∼1 per cent of the map rms.

3.1 The CMB component

We wanted to verify if the component extracted by FASTICA is indeed consistent with the CMB signal and the first figure of merit is the expected frequency scaling of the CMB between the two BEAST frequencies. BEAST data are in antenna temperature and CMB fluctuations $\delta T_{A,CMB}$ are related to brightness temperature fluctuation δT_{CMB} by

$$\delta T_{A,CMB}(\nu) = \frac{x^2 e^x}{(e^x - 1)^2} \delta T_{CMB},$$ (2)

where $x = h\nu/kT_{CMB}$. Assuming for the CMB a blackbody temperature $T_{CMB} = 2.725$ K (Mather et al. 1999), we expect for the CMB component a frequency scaling between 30 (*Ka*) and 41.5 (*Q*) GHz equal to 1.022.

After removing the sky regions strongly contaminated by Galactic emission, FASTICA recovers an astrophysical component with fre-

quency scaling quite different from that expected for CMB, as shown in Table 1. This is due to the high noise contribution, which affects also the reconstructed astrophysical signal. Furthermore, from Table 1 we can observe that results obtained with *t* function are in general worse than *p* and *g* results. Finally, increasing angular scale, with *p* and *g* the frequency scaling approaches the expected value in most of the cases. Nevertheless, the spatial pattern of the reconstructed astrophysical component resembles the *Q* map pattern, as shown in Fig. 1 for the 40-arcmin smoothing case.

After this first indication, we proceeded by verifying that reconstructed maps at different resolution are consistent one each other. After smoothing all maps down to 60 arcmin, we have calculated the correlation between maps with different original resolution, finding Spearman correlation coefficients $r_s > 0.8$ (with the exception of correlation between maps 30 and 60 arcmin obtained with *t* function, for which $r_s \sim 0.7$). This correlation indicates that FASTICA recovers the same astrophysical signal at every resolution. Furthermore, we observed that all the reconstructed maps have high spatial correlation with the *Q*-band map smoothed at the same resolution, with $r_s > 0.9$ except for *t* results at 40 arcmin ($r_s \sim 0.7$) and at 60 arcmin ($r_s \sim 0.6$). This is indeed expected since the S/N ratio is larger in *Q* band than in *Ka* band. Finally, we verified that there are no significant changes in the astrophysical component reconstruction when extending the Galactic cut. Indeed, reconstructed maps applying different cuts are consistent one each other ($r_s \sim 0.9$). Also the frequency scaling does not change significantly with the Galactic cut (see Table 1) and there is not a well-defined trend in the scaling variations with the cut extension. This points out that the Galactic contribution in the reconstructed astrophysical component is not relevant. Therefore, we are confident that FASTICA recovers a signal dominated by CMB anisotropies.

3.2 Testing results with Monte Carlo simulations

Given the poor-S/N ratio in the BEAST data, we prefer to test the performance of FASTICA by simulation. In order to analyse CMB reconstruction quality, we performed 100 Monte Carlo simulations in which sky signal is simulated, observed following BEAST observing strategy, reduced as the actual data and then analysed by FASTICA. We already demonstrated that foreground contribution is negligible and therefore we decided not to add any foreground templates. The CMB sky is generated according to the *WMAP* best-fitting power spectrum (Bennett et al. 2003) and convolved with a symmetric Gaussian beam with the BEAST angular resolution: 30 arcmin in *Ka* band and 23 arcmin in *Q* band. Maps are pixelized in HEALPix format (Górski et al. 1999) with $N_{side} = 512$. Observing these maps, we produced time-ordered data (TOD) for each BEAST channel from which we created maps in *Ka* and *Q* bands following the same reduction processing of the real BEAST data (see Meinhold et al. (2005), for map-making process details).
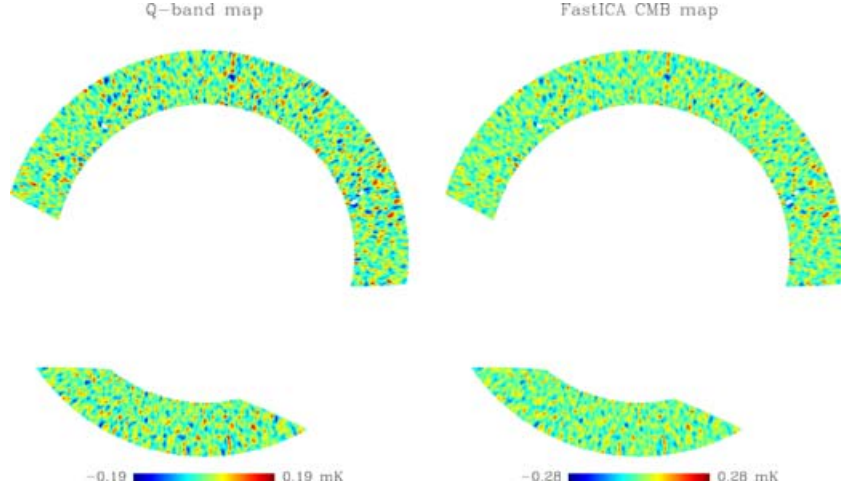
Figure 1. left: the BEAST *Q*-band map smoothed to 40 arcmin; right: the reconstructed astrophysical component (with *g* function). The Galactic plane is removed for $|b| \leqslant 17°\!5$.

As for instrumental noise simulation, we did not produce noise time streams for each of BEAST detectors, but we adopted a different recipe in order to have noise maps with the same statistical properties as the actual data.

We generated white noise realizations with the same rms per pixel of BEAST maps in the two bands. It is clear that this is not enough due to the non-negligible level of $1/f$ noise (e.g. Meinhold et al. 2005) which makes the noise clearly not-white. We made use of the 'difference' maps as derived by Meinhold et al. (2005) to extract the noise angular distribution. We then expanded in spherical harmonics both the white noise and the 'difference' maps obtaining the harmonic coefficients $a_{\ell m}^w$ and $a_{\ell m}^d$, respectively. These coefficients are combined according to

$$a_{\ell m}^s = \sqrt{\frac{\sum_m |a_{\ell m}^d|^2}{\sum_m |a_{\ell m}^w|^2}}\, a_{\ell m}^w, \tag{3}$$

and we then generated noise maps with these new $a_{\ell m}^s$ coefficients. In this way noise simulated maps have also the same angular power spectra as the actual processed BEAST maps. We repeated this procedure for each of the two BEAST frequency bands. Finally, after smoothing to 30-, 40- and 60-arcmin angular resolution, we added CMB and noise simulated maps together at each frequency, obtaining simulated BEAST maps. Subpixel noise effects are negligible due to the high angular resolution, and the smoothing reduces any possible residual effect. In Table 2, we report the S/N ratios of the simulated maps. We underline that simulated *Q* maps smoothed to 30 arcmin have the same S/N ratio estimated by Meinhold et al. (2005) for the BEAST 30-arcmin *Q* map derived with full processing of the data. This fact is a direct verification of the success of our recipe for noise simulations.

Subsequently, we applied FASTICA to the simulated maps, after removing the region with $|b| \leqslant 17°\!5$ as done for the actual data. For every run we derived correlation coefficients of both ICA maps with

the input CMB. Therefore, the ICA map of the two with the higher correlation coefficient is a possible CMB reconstruction.

Fig. 2 shows the relation between correlation coefficients and frequency scaling of the possible CMB reconstruction at the three different angular resolutions for the three non-quadratic forms assumed by ICA. It is interesting to note that in correspondence of the expected CMB frequency scaling (1.022), we observe the higher correlation coefficients and then the best recovered CMB. We therefore use frequency scaling as a figure of merit for the CMB reconstruction. Furthermore, we observe from Fig. 2 that increasing angular resolution, increases also values of the correlation: CMB reconstruction becomes better. This is expected because the S/N ratio increases with angular resolution (see Table 2).

Finally, we used this relationship between correlation and frequency scaling to establish which CMB reconstructions are reliable. For every resolution, we selected the minimum correlation value that characterizes a good reconstruction. This correlation coefficient r_s corresponds to a maximum value of frequency scaling *s*. In Table 3, we report the chosen values of correlation coefficient and frequency scaling (selecting regions near the peaks in Fig. 2) and the number of 'good' recovered CMB maps. As already noted in previous works (e.g. Maino et al. 2002, 2003), FASTICA results with *t* function are the worst, while *g* performs better in the astrophysical context. Increasing angular scale increases the number of 'good' CMB reconstructions and decreases the differences between *p*, *g* and *t*.

Looking at the CMB recovered from the data, we verify that the frequency scalings reported in Table 1 lie within the range of values that identify at every resolution a 'good' reconstruction, with the exception of *t* results at 40 and 60 arcmin. This is a further indication of the fact that FASTICA is able to extract reliable CMB signal.

4 NORMALIZATION OF THE CMB COMPONENT

In general, FASTICA recovers a copy of the original signal i.e. it is not able, in principle, to recover the variance of the underlying sources. Therefore, we have to normalize the CMB component recovered from BEAST data. Generally, we can derive the right normalization factor directly from the FASTICA outputs, but in this case, due to the

Table 2. Simulated maps S/N ratios

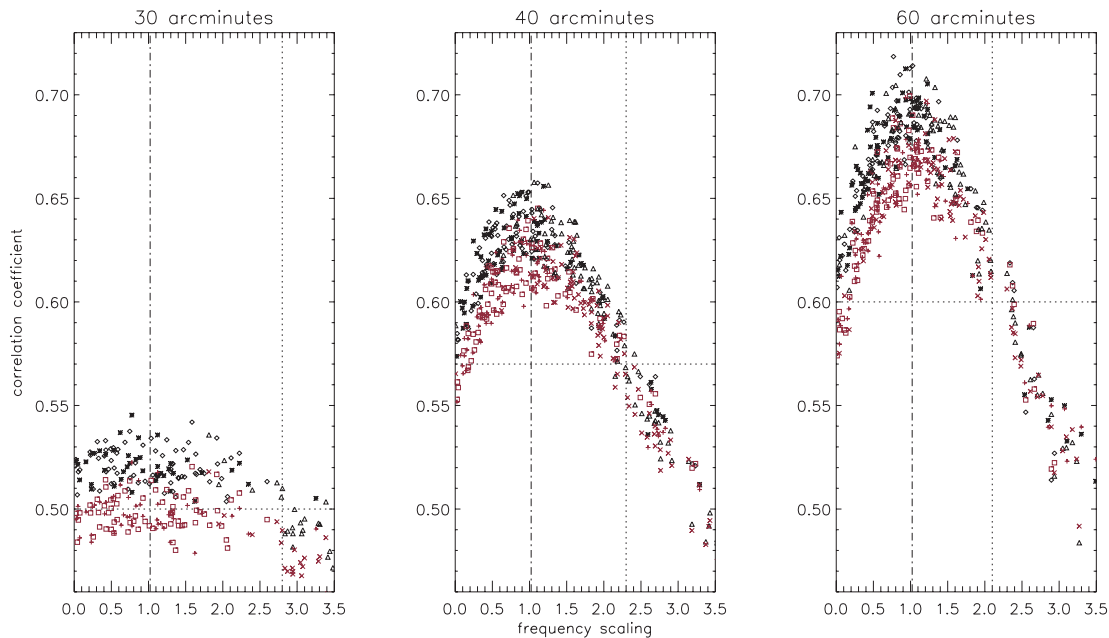| S/N (arcmin)	*Ka*	*Q*
30′	∼0.09	∼0.57
40′	∼0.28	∼0.81
60′	∼0.33	∼0.85

Figure 2. Correlation between ICA CMB and simulated CMB in *Ka* (plus sign = *p*, square = *g*, 'x' = *t*) and *Q* band (asterisk = *p*, diamond = *g*, triangle = *t*) towards recovered frequency scaling at 30, 40 and 60 arcmin. Dot–dashed lines show the expected scaling (1.022). Dotted lines indicate the minimum correlation and the maximum scaling for a good CMB reconstruction. We can also observe that correlation with CMB-*Q* map is greater than with CMB–*Ka* map.

Table 3. Number of 'good' CMB reconstructions from 100 simulated maps for each angular scale using *p*, *g* and *t* function in the FASTICA algorithm. See the text for explanation.

30 arcmin	*p*	*g*	*t*
$r_s > 0.50$	43	70	8
$s < 2.8$	42	70	6
40 arcmin	*p*	*g*	*t*
$r_s > 0.57$	69	82	70
$s < 2.3$	69	82	71
60 arcmin	*p*	*g*	*t*
$r_s > 0.60$	76	82	76
$s < 2.1$	76	79	74

linear within a frequency scaling s_{max} and a normalization factor N_{max}. Such values decrease when angular scale increases since FASTICA performs better (see Table 3) and scalings identifying a 'good' CMB reconstruction are within s_{max}. Furthermore, when the CMB component has the expected frequency scaling, it has also the right normalization, with scalefactor equal to 1.

In Fig. 3, we also report the frequency scalings obtained from BEAST data at the three angular resolutions and for the three non-quadratic functions. We derived the normalization factor by simple linear interpolation of this relation in the points corresponding to the actual frequency scalings.

Finally, we observe that this relation does not depend on the functions *p*, *g* and *t*, and not even on angular resolution for scaling smaller than the theoretical one as shown in Fig. 4.

5 POWER SPECTRUM

We estimated the angular power spectrum of the FASTICA CMB component from BEAST data and compared it with that derived by O'Dwyer et al. (2005) for the analysis of *Q*-band BEAST data. We extracted the spectrum choosing an angular resolution of 40 arcmin. This is a good compromise between S/N ratio and signal level which is affected by the 10-Hz high-pass filter applied to the data. We considered the more conservative Galactic cut ($|b| \leqslant 17.5°$) and used the *g* function in the ICA algorithm which has the better recovered frequency scaling (see Table 1).

To extract the CMB power spectra, we adopted the Monte Carlo Apodised Spherical Transformation Estimator (MASTER) method (Hivon et al. 2002) that was also used by O'Dwyer et al. (2005). MASTER returns a binned pseudo-C_ℓ estimator allowing for debiasing the power spectrum for the effects specific of the experimental CMB observation, such as sky cut, scanning strategy, data processing and instrumental noise. This is expressed by the
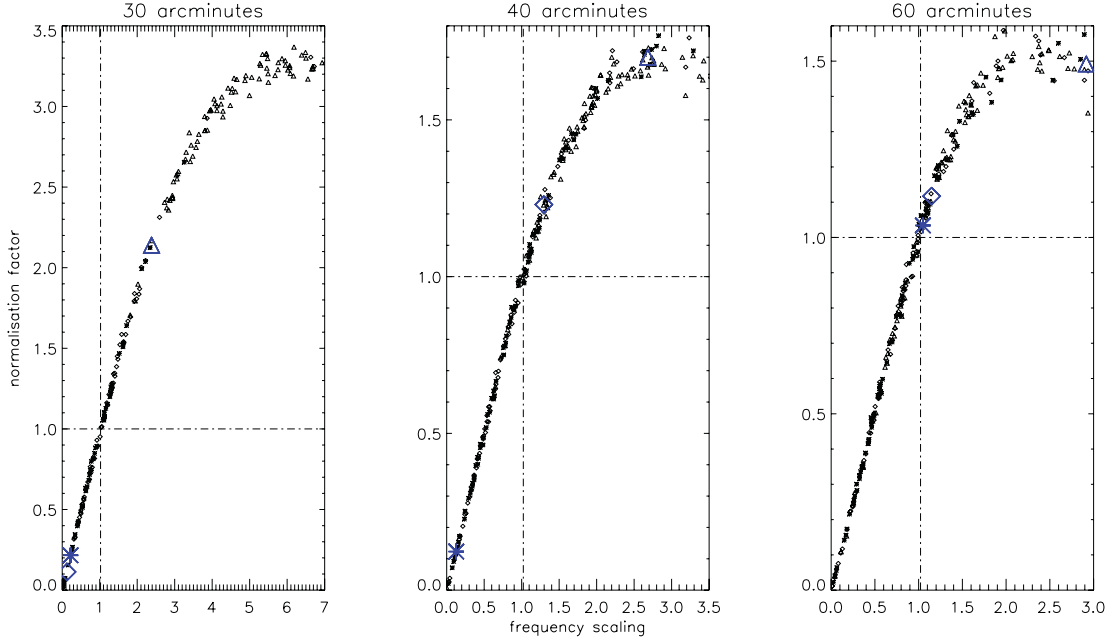
poor-S/N ratio, we must again use our Monte Carlo simulations. In fact, for each CMB recovered from simulations the scalefactor is just the ratio between reconstructed and input CMB maps rms. The output CMB map is in *Ka*-band antenna temperature, and we compare it with the simulated CMB map in *Ka* band. However, noise in the reconstructed CMB is quite important and we have to estimate and subtract it (at least in terms of rms). Although the FASTICA algorithm is highly non-linear, the data model is linear i.e. sources are obtained with a linear combination of the input data. In this way, we can quite easily estimate the noise contribution in the reconstructed components by exploiting the separation matrix **W** elements pertinent to the CMB component. We then subtracted, for each simulation, noise rms from the output CMB rms to obtain the exact recovered CMB rms to compare with the input CMB rms.

Results are shown in Fig. 3, where normalization factor is reported as function of the frequency scaling at the three different angular resolutions. There is a clear relationship between normalization factor and frequency scaling. Indeed, this relation is almost

Figure 3. Normalization factor as a function of the frequency scaling for 30, 40 and 60 arcmin. Dot–dashed lines indicate normalization factor equal to 1 and the expected frequency scaling. The bigger symbols show the interpolation with the frequency scalings of the CMB recovered from BEAST data, cutting the Galactic plane for $|b| \leqslant 17.5°$ and using p (asterisks), g (diamonds) and t (triangles) function.
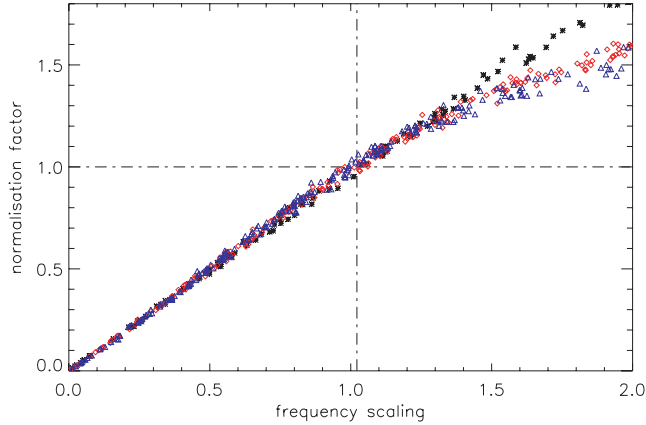

Figure 4. Normalization factor as a function of frequency scaling for 30 (asterisks), 40 (diamonds) and 60 arcmin (triangles).

following data model:

$$\tilde{C}_\ell = \sum_{\ell'} M_{\ell\ell'} F_{\ell'} B_\ell^2 C_{\ell'}^{\text{th}} + \langle N_\ell \rangle, \qquad (4)$$

where $\tilde{C}_\ell$ is the observed power spectrum, C_ℓ^{th} is the theoretical one. The B_ℓ^2 term includes both instrumental and pixel window functions and the kernel $M_{\ell\ell'}$ accounts for the mode–mode coupling between different modes due to the incomplete sky coverage and depends on the actual shape of the observed sky region (so it can be computed once for all). The other terms are calibrated against Monte Carlo simulations. In particular, with simulations of CMB only observations we compute the instrumental transfer function F_ℓ, which accounts for data processing effects. Instrumental noise only simulations are needed to estimate the average noise angular power spectrum $\langle N_\ell \rangle$, while from simulated skies (CMB + noise)

we derive errors on our final power-spectrum estimation (see Hivon et al. (2002), for details).

For a proper application of MASTER to a FASTICA CMB map, we must take into account that an ICA CMB map is indeed a linear combination of two data maps: the one in *Ka* band and the other in *Q* band, i.e. $\mathbf{y}_{\text{CMB}} = w_{Ka}\mathbf{x}_{Ka} + w_Q\mathbf{x}_Q$, where the weights w_{Ka} and w_Q are derived from the ICA separation matrix **W**. In general, due to the different S/N ratios, we have obtained $w_Q > w_{Ka}$ (for example, in the chosen case we have $w_{Ka} \sim 0.20$ and $w_Q \sim 1.04$), however, the ICA CMB power spectrum is affected by experimental observation effects in both the bands. In order to evaluate such effects, we made use of the Monte Carlo simulations already performed at 40 arcmin. First, we used simulated *Ka*- and *Q*-band CMB to estimate the instrumental transfer functions for *Ka* and *Q* bands separately, F_ℓ^{Ka} and F_ℓ^Q, respectively. We then computed the final ICA transfer function as $F_\ell = w_{Ka}^2 F_\ell^{Ka} + w_Q^2 F_\ell^Q$. Instrumental noise, and its angular power spectrum, in the reconstructed CMB component is obtained in a similar manner: we use the same coefficients w_{Ka} and w_Q to properly combine the *Ka*- and *Q*-band instrumental noise realizations. Finally, the same weights are used in signal plus noise simulations in order to derive final error on the MASTER power spectrum.

We extracted the binned power spectrum choosing the same multipole bins used by O'Dwyer et al. (2005), with $\Delta\ell = 55$. We estimated the ICA power spectrum for multipoles $\lesssim$400 since signal is significantly suppressed at higher multipoles due to the selected 40-arcmin smoothing.

Finally, since FASTICA does not recover a CMB signal with the right variance, we normalized the spectrum using the scalefactor derived from interpolation of the 'normalization factor–frequency scaling' relation, as described in the previous section (see Fig. 3).

The resulting 40-arcmin FASTICA CMB power spectrum is shown in Fig. 5, compared with the 23-arcmin *Q*-band map power spectrum estimated by O'Dwyer et al. (2005) and with the best-fitting *WMAP* model. The agreement between the spectra is good. In particular,
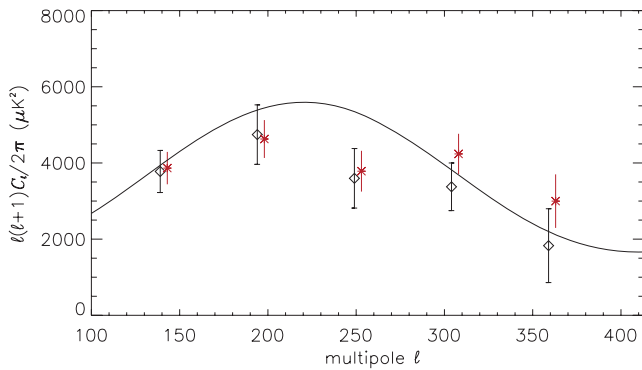
Figure 5. CMB power spectra from BEAST data: stars show the spectrum extracted from FASTICA 40-arcmin CMB map, diamonds show the 23-arcmin *Q*-band map spectrum (O'Dwyer et al. 2005). ICA spectrum is shifted by $\Delta\ell = 4$ for clarity. Solid line is the best-fitting *WMAP* power spectrum.

Table 4. The BEAST C_ℓ and 1σ error values (in μK^2).

bin $\ell_{\min}-\ell_{\max}$	FASTICA map $\ell(\ell+1)C_\ell/2\pi$	1σ error	Q map $\ell(\ell+1)C_\ell/2\pi$	1σ error
139–193	3865	±425	3776	±552
194–248	4628	±497	4744	±781
249–303	3783	±535	3597	±782
304–358	4237	±528	3374	±625
359–413	2997	±703	1829	±969

the two BEAST spectra agree within 1σ. In Table 4, we report the C_ℓ and associated 1σ errors for the two BEAST power spectra. Furthermore, both from Fig. 5 and Table 4, we can observe that ICA spectrum error bars are smaller than those of the *Q*-band power spectrum. This is due to the smoothing at 40 arcmin, which reduces the noise contribution.

The spectra agreement is a strong indication of the suitability of the FASTICA CMB signal, and also of the goodness of the adopted normalization procedure.

6 CRITICAL DISCUSSION AND CONCLUSION

In this paper, we applied FASTICA algorithm to real CMB data from the BEAST experiment. This is a ground-based experiment operating from the UC White Mountain Research Station (CA) at an altitude of 3.8 km that produced partial sky maps in two frequency bands (*Ka* and *Q*) with angular resolution of 30 and 23 arcmin, respectively.

One of the FASTICA requirements is that the instrumental noise has to be Gaussian and uniformly distributed on the sky. This is not the case for BEAST, which clearly shows $1/f$ noise and non-uniform integration time due to the observing strategy. The $1/f$ noise has been accounted for by applying a high-pass filter to the TOD in the map-making process. This of course alleviates the impact of non-white noise but also reduces sky signal on large angular scales. Furthermore, the S/N ratio, as estimated from 'difference' maps by Meinhold et al. (2005), is quite poor being $\sim$0.11 for *Q* band and even lower in *Ka* band.

Another limitation for FASTICA applicability is that different frequency channels have to be at the same angular resolution. This forces us to further convolve our data set. We choose three different values for resolution: 30, 40 and 60 arcmin. We did not apply a more

aggressive smoothing since the high-pass filter effect on data is a clear suppression of signal on larger scales. Smoothing data allows us to reach a slightly better S/N ratio which helps in the application of FASTICA.

All these constraints have the consequence that FASTICA always extracts from BEAST data, one physical component while the other is clearly noise related. Furthermore, in order to extract a CMB component, we have to cut out the Galactic plane where Galactic emission is dominating over CMB since otherwise this would prevent us from properly reconstructing CMB. Nevertheless, after Galactic cut, FASTICA recovers a CMB-like component, but with frequency scalings (Table 1) quite different from the theoretical one. This is again due to the relatively high instrumental noise, which alters CMB reconstruction. Despite this first bad indication, with further analysis, we verified that this component is indeed dominated by CMB anisotropies.

In order to test our CMB results quality, we ran FASTICA on 100 Monte Carlo simulations of *Ka*- and *Q*-band data at the three selected angular resolutions. These have been simulated by creating fake CMB skies with angular power spectrum from the best-fitting model from *WMAP* (Bennett et al. 2003), observing these skies according to BEAST scanning strategy and reducing data with the same pipeline applied to real data. We finally superimposed instrumental noise with the same statistical and spatial properties as the actual data. We derived correlation coefficients between CMB ICA maps with the input CMB and studied the relation between these coefficients and the recovered scaling frequency, in order to use scaling as a figure of merit. For every resolution, we selected the maximum scaling allowed for a 'good' CMB reconstruction and the comparison of these values with the results out of BEAST data confirms that FASTICA indeed recovers a reliable CMB component. Furthermore, the relation shows the increasing reconstruction quality with angular scale, since the increasing S/N ratio, and the different FASTICA performance with the three non-quadratic functions, with the better and the worse results obtained using *g* and *t* functions, respectively. This final indication agrees with previous works (Maino et al. 2002, 2003).

Since FASTICA is not able to recover the variance of the independent components (it recovers a 'copy' of the independent underlying components), we again used Monte Carlo simulations to obtain a normalization procedure for the CMB component. In fact, in this case the scalefactor is just the ratio between output and input CMB rms. For each resolution, we found a clear relation between scalefactor and frequency scaling that is almost linear within certain values of scaling and normalization factor. The decreasing of such values with angular scale indicates again the corresponding improvement of FASTICA performance due to the better S/N ratio. Furthermore, the relation does not depend on the non-quadratic function and shows that those CMB reconstructions with the expected frequency scaling have also the correct normalization (e.g. equal to 1). The normalization factors for FASTICA results out of BEAST data are derived by interpolation of this relation at the derived frequency scalings.

Finally, we extracted the FASTICA CMB angular power spectrum adopting a MASTER approach (Hivon et al. 2002) and normalized it with the proper scalefactor. We found a very good agreement with our results and the best-fitting *WMAP* model and also with the spectrum estimated from the BEAST *Q*-band map (O'Dwyer et al. 2005), although on a limited multipole range because of the extra smoothing applied to the data. This spectra agreement confirms the reliability of the CMB extracted by FASTICA and validates our normalization procedure.

Our analysis, together with that on DMR data performed by Maino et al. (2003), confirms the very good performance of blind algorithms like FASTICA in extracting a CMB component even from noisy data on a small patch of the sky like BEAST ones. Therefore, we think that blind algorithms are valid tools for present and future CMB experiments providing information on the independent component in the actual observed sky signal which could be used to feed much more complex algorithm like MEM. This is particularly relevant for future CMB polarization experiments, where we will be forced to work with low-S/N ratios and where our knowledge of polarization for foregrounds is still poor (Stivoli et al. 2005).

ACKNOWLEDGMENTS

REFERENCES

Baccigalupi C. et al., 2000, MNRAS, 318, 767
Bennet C. L. et al., 2003, ApJS, 148, 97
Bouchet F. R., Prunet S., Sethi S. K., 1999, MNRAS, 302, 663
Childers J. et al., 2005, ApJS, 158, 124
Comon P., 1994, Signal Process., 36, 287
Figueiredo N. et al., 2005, ApJS, 158, 118
Górski K. M., Hivon E., Wandelt B. D., 1999, in Banday A. J., Sheth R., Da Costa L. N., eds, Evolution of Large Scale Structure: from Recombination to Garching. PrintPartners Ipskamp, Enschede, NL
Hivon E., Górski K. M., Netterfield C. B., Crill B. P., Prunet S., Hansen F., 2002, ApJ, 567, 2
Hobson M. P., Jones A. W., Lasenby A. N., Bouchet F. R., 1998, MNRAS, 300, 1
Hyvärinen A., Oja E., 1997, Neural Comput., 9, 1483
Hyvärinen A., 1999, IEEE Signal Process. Lett., 6, 145
Hyvärinen A., Oja E., 2000, Neural Netw., 13, 411
Leitch E. M., Kovac J. M., Halverson N. W., Carlstrom J. E., Pryke C., Smith M. W. E., 2005, ApJ, 624, 10
Maino D. et al., 2002, MNRAS, 334, 53
Maino D., Banday A. J., Baccigalupi C., Perrotta F., Górski K. M., 2003, MNRAS, 344, 544
Mather J. C., Fixsen D. J., Shafer R. A., Mosier C., Wilkinson D. T., 1999, ApJ, 512, 511
Meinhold P. R. et al., 2005, ApJS, 158, 101
Mejía J. et al., 2005, ApJS, 158, 109
O'Dwyer I. J. et al., 2005, ApJS, 158, 93
Prunet S., Teyssier R., Scully S. T., Bouchet F. R., Gispert R., 2001, A&A, 373, L13
Stivoli F., Baccigalupi C., Maino D., Stompor R., 2005, MNRAS, submitted (astro-ph/0505381)
Stolyarov V., Hobson M. P., Ashdown M. A. J., Lasenby A. N., 2001, MNRAS, 336, 97
Tegmark M., Efstathiou G., 1996, MNRAS, 281, 1297

This paper has been typeset from a TEX/LATEX file prepared by the author.